AD-A161 021 NUMERICAL COMPUTATION OF HYPERSONIC LAMINAR NEAR-WAKE FLOW VIA NAVIER-STO (U) LOCKHEED MISSILES AND SPACE CO INC PALO ALTO CA PALO ALTO RES Y TASSA ET AL. JUL 85 1/1

UNCLASSIFIED N00014-82-C-0690 F/G 20/4 NL

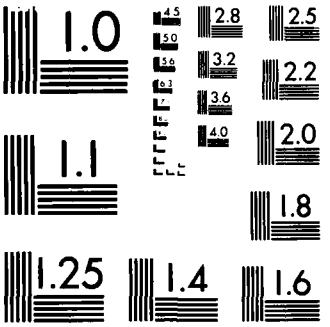

(12)

AIAA'85

AIAA-85-1672
Numerical Computation of Hypersonic Laminar Near-Wake Flow via Navier-Stokes Solver

Yehuda Tassa and Raul J. Conti
Lockheed Palo Alto Research Laboratory
Palo Alto, California

Contract N00014-82-C-0690

AIAA 18th Fluid Dynamics and Plasmadynamics and Lasers Conference

July 16-18, 1985 / Cincinatti Ohio

NUMERICAL COMPUTATION OF HYPERSONIC LAMINAR NEAR-WAKE FLOW VIA NAVIER-STOKES SOLVER

Yehuda Tassa* and Raul J. Conti†

Lockheed Palo Alto Research Laboratory
Palo Alto, California

Abstract

Numerical solutions of the Navier-Stokes equations are obtained for laminar hypersonic near-wake flow behind cones at zero angle of attack. Numerical simulations are presented for a cone with a 7-degree half-angle. The study includes three values of free-stream Mach number (4.32, 6.32, 10.0) and four values of Reynolds number ranging from 21500 to 172000 referenced to base diameter. The numerical scheme is patterned after the Alternating Direction Implicit method of Beam and Warming, with modification to include finite-volume discretization and spatially variable time step for accelerating convergence to steady state. Comparisons are made with experimental data for base pressure, length of the recirculating region, and general flow-field structure. Effects of Mach and Reynolds numbers on the laminar near-wake flowfield structure are reported.

Introduction

Considerable amount of research, both theoretical and experimental, has been devoted toward understanding the complex structure of hypersonic near-wake flows. Early interest focused on predicting base pressure or base drag. More recently, effort has been directed toward understanding the hypersonic near-wake flow structure since it plays an important role in the development of the far wake. Application of the time-dependent, compressible full Navier-Stokes equations to the hypersonic near-wake flow problem is very attractive because it has the potential for complementing the simplified or "component" theoretical models, while circumventing the persistent problems of support and probe interference that plague the experimental work. This study is concerned with the effects of Mach and Reynolds numbers on the structure of hypersonic laminar near-wake flows. Laminar flows are the first choice because the numerical solutions are not clouded by the uncertainties of turbulence modeling. Furthermore, the present study establishes a promising approach for more detailed investigation of the near-wake structure, and for evaluation of the spurious effects introduced by model supports and probes used in wind-tunnel tests.

The brief review that follows concentrates on laminar wakes created by cones in supersonic or hypersonic flight. Crane[1] has reviewed theoretical and experimental work on supersonic wakes, and he traces the development of theoretical models from the classical paper by Chapman[2], who considered a simple inviscid model of flow about a "dead-air" region aft of the body (see Fig. 1). In reality, viscous effects are important, and other shocks may appear, such as the lip shock associated with flow recompression near the base corner[3,4]. Some of the flow models are "component" models that break down the wake into separate but interacting regions or features, each more tractable than the whole. Thus, Baum[3] investigated the boundary layer upstream of the corner, Ohrenberger and Baum[5], and Weiss[6] concentrated on the near wake, and Zeiberg and Bleich[7] studied the region beyond the neck of the wake. Dash[8] and co-workers have extended a fam-

* Staff Scientist, Member AIAA

† Sr. Staff Scientist, Member AIAA

ily of component models to wakes, jets and plumes.

The experimental studies of near wakes include flight tests, ballistic-range tests, and wind-tunnel tests. The flight tests reported by Cassanto[9] and Bulmer[10] include base pressure and heat transfer to the body. Photographs taken in ballistic ranges by Lyons *et al*[11], Koch[12], Levensteins and Krumins[13] and others provide details of the wake geometry and shock location, as well as information on transition to turbulent flow (see Fig. 2). Wind-tunnel experiments are complicated by the problem of support interference. Dayman[14] pointed out that even the smallest wire supports can have dramatic effects on the structure of the near wake. This conclusion is supported by the experience of many others with all types of supports. To circumvent this problem a number of experiments have been performed with magnetically supported models[15-20]. These studies are attractive from the standpoint of support interference, but they are not free from tunnel and probe interference, as will be explained when discussing the present results, which are compared with the experiments of McLaughlin *et al*[18] and Blankson and Finston[20].

Correlations of various features of the near wake have been supplied by several authors to check their results or to predict needed information, such as base pressure,[10,21,22] wake transition,[23,24] the end of the recirculation region[25] or the location of the separation line[26-28].

Numerical simulation by means of Navier-Stokes techniques has been applied to projectile wakes by Sahu *et al*[29], by Deiwert[30] and by Thomas *et al*[31]. Reklis *et al*[32] show preliminary results for the wake of a sharp cone in hypersonic flight; Reklis and Conti[33] investigated the effects of Reynolds number at Mach 6.3. The present investigation extends the latter work with more accurate results, and a study of Mach number effects.

Mathematical Formulation

The selected ranges of Mach and Reynolds numbers used in this numerical study justify the assumption of laminar flow throughout the near wake. This is illustrated in Fig. 2, where those ranges are compared with various transition data and correlations. Hence the classical Navier-Stokes equations provide a realistic mathematical model for hypersonic laminar near-wake flow problems.

We can write the three-dimensional unsteady compressible Navier-Stokes equations in strong conservative form in a Cartesian coordinate system as

$$\mathbf{q}_t + \mathbf{f}_x + \mathbf{g}_y + \mathbf{h}_z = R_e^{-1}(\mathbf{\Gamma}_x + \mathbf{\Theta}_y + \mathbf{\Omega}_z) \quad (1a)$$

where

$$\mathbf{q} = [\rho, \rho u, \rho v, \rho w, \rho\epsilon]^T$$

$$\mathbf{f} = [\rho u, (p/\gamma + \rho u^2), \rho uv, \rho uw, u(p/\gamma + \rho\epsilon)]^T$$

$$\mathbf{g} = [\rho v, \rho vu, (p/\gamma + \rho v^2), \rho vw, v(p/\gamma + \rho\epsilon)]^T$$

$$\mathbf{h} = [\rho w, \rho wu, \rho wv, (p/\gamma + \rho\epsilon)]^T.$$

The equation of state for a thermally and calorically perfect gas

$$c^2 = p/\rho = T = \gamma(\gamma - 1)(\epsilon - V^2/2) \quad (1b)$$

is required to form a closed system. In equations (1) u, v, w represent the components of the velocity $\mathbf{V}$ along the coordinate directions x, y, z respectively, p represents the pressure, ρ the density, and ϵ the total (internal plus kinetic) specific energy. Equation (1a) is expressed in non-dimensional form, with reference values for the pressure, density, temperature and viscosity taken as their free-stream values; the reference speed is the free-stream speed of sound; the reference energy is the square of the free-stream speed of sound; the reference length is the diameter of the base of the cone; the reference time is constructed from the reference speed and length, and the Reynolds (R_e) and Mach (M) numbers are based on these reference values.

To enhance the numerical accuracy of boundary conditions, a generalized coordinate transformation of the governing equations is employed, while still retaining the strong conservation form. The boundary-conforming curvilinear coordinate system is subjected to the following time-dependent transformation,

$$x, y, z, t \Longleftrightarrow \xi, \eta, \varsigma, \tau \qquad (2)$$

$$\begin{aligned} \xi &= \xi(x, y, z, t) \\ \eta &= \eta(x, y, z, t) \\ \varsigma &= \varsigma(x, y, z, t) \\ \tau &= t, \end{aligned}$$

yielding the following system of equations:

$$\boldsymbol{q}_\tau + \boldsymbol{f}_\xi + \boldsymbol{g}_\eta + \boldsymbol{h}_\varsigma = R_e^{-1}(\boldsymbol{\Gamma}_\xi + \boldsymbol{\Theta}_\eta + \boldsymbol{\Omega}_\varsigma) \quad (3)$$

where

$$\begin{aligned} \boldsymbol{q} &= J\mathbf{q} \\ \boldsymbol{f} &= J(\xi_t\mathbf{q} + \xi_x\mathbf{f} + \xi_y\mathbf{g} + \xi_z\mathbf{h}) \\ \boldsymbol{g} &= J(\eta_t\mathbf{q} + \eta_x\mathbf{f} + \eta_y\mathbf{g} + \eta_z\mathbf{h}) \\ \boldsymbol{h} &= J(\varsigma_t\mathbf{q} + \varsigma_x\mathbf{f} + \varsigma_y\mathbf{g} + \varsigma_z\mathbf{h}) \\ \boldsymbol{\Gamma} &= J(\xi_x\boldsymbol{\Gamma} + \xi_y\boldsymbol{\Theta} + \xi_z\boldsymbol{\Omega}) \\ \boldsymbol{\Theta} &= J(\eta_x\boldsymbol{\Gamma} + \eta_y\boldsymbol{\Theta} + \eta_z\boldsymbol{\Omega}) \\ \boldsymbol{\Omega} &= J(\varsigma_x\boldsymbol{\Gamma} + \varsigma_y\boldsymbol{\Theta} + \varsigma_z\boldsymbol{\Omega}), \end{aligned}$$

and J is the Jacobian of the inverse transformation (2)

$$J = \partial(x, y, z)/\partial(\xi, \eta, \varsigma).$$

The column vectors $\boldsymbol{\Gamma}, \boldsymbol{\Theta}, \boldsymbol{\Omega}$ can be conveniently decomposed into three terms, each one containing derivatives of the flow variables with respect to only one coordinate (indicated by a superscript in parentheses) *i.e.*,

$$\begin{aligned} \boldsymbol{\Gamma} &= \boldsymbol{\Gamma}^{(\xi)} + \boldsymbol{\Gamma}^{(\eta)} + \boldsymbol{\Gamma}^{(\varsigma)} \\ \boldsymbol{\Theta} &= \boldsymbol{\Theta}^{(\xi)} + \boldsymbol{\Theta}^{(\eta)} + \boldsymbol{\Theta}^{(\varsigma)} \\ \boldsymbol{\Omega} &= \boldsymbol{\Omega}^{(\xi)} + \boldsymbol{\Omega}^{(\eta)} + \boldsymbol{\Omega}^{(\varsigma)}. \end{aligned}$$

The detailed expansions of the terms in the right-hand sides of these equations are given by Thomas[34].

Equations (3) and (1b) are the full governing equations; for the present application to conical vehicles the streamwise coordinate is ξ, the circumferential coordinate is η, and the cross-stream coordinate is ς. Since the flow is axisymmetric, derivatives of the flow variables with respect to η are zero. However, some of the metric terms give non-zero contributions in this direction, giving rise to a source-like term in the left-hand side of (3). This term was evaluated analytically, following Nietubicz *et al*[35]. Some of the transport terms in the right-hand side of (3) were neglected for convenience, namely $\boldsymbol{\Theta}, \boldsymbol{\Gamma}^{(\eta)}$, and $\boldsymbol{\Omega}^{(\eta)}$. Equation (3) then reduces to

$$\boldsymbol{q}_\tau + \boldsymbol{f}_\xi + \boldsymbol{h}_\varsigma + \mathrm{G} =$$

$$R_e^{-1}[\boldsymbol{\Gamma}_\xi^{(\xi)} + \boldsymbol{\Gamma}_\xi^{(\varsigma)} + \boldsymbol{\Omega}_\varsigma^{(\xi)} - \boldsymbol{\Omega}_\varsigma^{(\varsigma)}] \qquad (4)$$

where G represents the metric source term. In the "thin-layer" approximation[36] only the term $\boldsymbol{\Omega}_\varsigma^{(\varsigma)}$ on the right-hand side of (4) is retained. In the present application all terms of (4) were retained, and the "cross-derivative" terms $\boldsymbol{\Gamma}_\xi^{(\varsigma)}$ and $\boldsymbol{\Omega}_\varsigma^{(\xi)}$ were found to be essential to achieve convergence. This is attributed to the complex character of the flowfield, which features boundary layers running in the ξ and the ς directions, recirculating flow, and multiple stagnation points. The cross-derivative terms are cumbersome to handle implicitly, and were instead differenced explicitly, without undue ill effects.

Numerical Method

The numerical scheme implemented is patterned after the Alternate Direction Implicit (ADI) method of Beam and Warming[37]. Several modifications have been made to the numerical algorithm, including the finite-volume discretization of Thomas and Lombard[38] and

central-difference formulas that are second-order-accurate spatially. Conservative artificial dissipation terms have been added in order to suppress the high-frequency components that appear in regions of severe pressure gradient, such as the neighborhood of shock waves. An explicit fourth-order term has been added to the right-hand side of the difference equations, and an implicit second-order term has been added to the left-hand side of the discretized equations. Also, to accelerate the convergence of the solution to steady state, a spatially variable time step has been incorporated. In this procedure each cell in the computational domain is advanced to steady state at the maximum local time step allowed by the linear stability analysis. On grids for viscous flow, where grid lines are highly stretched normal to the surface, the time steps can vary by several orders of magnitude. This fact dramatically affects the convergence rate of the solution.

Mesh System

A body-fitted coordinate system is desirable, since boundary surfaces in physical space are mapped onto rectangular surfaces in computational space, to allow more accurate treatment of boundary conditions. The physical space, which is L- shaped, requires non-uniform grid distribution to exploit the important length scales involved in this flow problem. The transformed space retains the same topology (L-shaped) but with uniform discretization.

Boundary Conditions

The boundary conditions are as follows (refer to Fig. 3): Adiabatic-wall and no-slip boundary conditions are implemented explicitly along the side of the cone (A-F in Fig. 3), and on its base (E-F). Upstream of the base, along a normal to the axis, (A-B) a fixed inflow condition given by a forebody solution of the viscous flow over a sharp cone, obtained in the manner described by Reklis *et al*[82]. Along the axis (E-D) explicit symmetry boundary conditions are used; along a normal to the axis, at the downstream end of the flowfield (D-C) an implicit supersonic outflow condition; and on the upper side of the flowfield (B-C) a fixed shock condition. The shock is simply a rectilinear continuation of the bow shock created by the sharp cone, and is unaffected by the base flow ahead of the leading edge of the base expansion. The shock-expansion interaction and its downstream effect on the flowfield are neglected on the grounds that they are of little consequence to the near-wake region.

Results

The numerical solutions in the present paper address the effects of Mach and Reynolds numbers on the structure of laminar near-wake flows at supersonic and hypersonic speed. The computations simulate the laminar near wake behind a cone having a half-angle of 7 degrees, and adiabatic wall. The flow conditions investigated in the present paper cover a range of Mach and Reynolds numbers as given in Table 1.

Table 1
Flow Condition Matrix

Re_d	M=4.32	M=6.32	M=10.0
21,500	X		
43,000	X	X	
86,000	X	X	X
172,000		X	X

The numerical solutions at Mach numbers of 4.32 and 6.32 are compared with the experimental data of McLaughlin *et al*[18] and Blankson and Finston [20] respectively, as discussed below. The computational grid used in all present calculations is a 92×58 mesh, with 92 grid lines in the axial direction and 58 grid lines in the direction normal to the axis. Non-uniform grid distribution was used in both directions. The mesh system extends about 5

diameters downstream of the base. A typical mesh system used in the present calculations is shown on Fig. 4.

Related Experiments

Experimental investigation of the near wake of models suspended in wind tunnels is hampered by significant interference from the suspension system, as indicated by Dayman[14]; on the other hand, the information provided by free-flight experiments, although free from support interference, is severely limited by the experimental environment. In an effort to circumvent the support interference problem, a few investigators have resorted to magnetic suspension of models, notably Murman[16], McLaughlin *et al*[18], and Blankson and Finston[20]. Data from the latter two investigations, taken in the same wind tunnel at different Mach numbers, were used in the present study to validate the numerical simulations. These data consist mainly of Pitot probe measurements and recovery temperature measurements. McLaughlin also measured static pressure with two types of probe. All these data are essentially free from support interference, but are apparently affected by extraneous tunnel effects. For instance, the Blankson data were taken in an accelerating stream (nominally at Mach 6.32) that ranged from Mach 6.45 to 6.65 along the wake under study. The angle of the bow shock, deduced from the Pitot data, is 10.8 degrees near the base of the model. This value is low compared with the theoretical value of 11.6 degrees for inviscid conical flow, and the numerical result of 12.0 degrees obtained in the present study. These effects hamper direct comparison of presure and temperature profiles. Therefore, quantitative comparisons are limited to overall quantities such as base pressure and location of the rear stagnation point. Qualitative comparison of wake features, as well as profiles of Pitot pressure and total temperature, which were measured experimentally, show good agreement with the present numerical simulations.

Accuracy

The choice of a proper grid that resolves all the essential physical features of a given flow problem is an important issue that needs to be addressed in any numerical simulation. A flowfield simulation with an excessively large number of mesh points requires unnecessary computing time, whereas an insufficient number of mesh points may degrade the accuracy significantly. The effect of grid resolution on the numerical accuracy has been studied in the present work. The Blankson[20] experimental data at Mach number of 6.32 and Reynolds number of 86000 has been selected as a bench mark. In the computations, 58 mesh points were distributed non-uniformly in the radial direction, and this number was held fixed. The axial mesh was refined successively to yield three mesh systems of 46×58, 92×58, and 135×58 points. It was found that the location of the rear stagnation point is sensitive to low streamwise mesh resolution.

Table 2
Effect of Mesh Resolution on Location of Rear Stagnation Point

Mesh Size	X_{STG}/D
46×58	2.40
92×58	1.40
135×58	1.49

Table 2 shows the axial location of the rear stagnation point for the various grids. It is clear that the 46×58 mesh is not sufficient to resolve the near wake structure and leads to significant error. The solution for the 92×58 mesh compares well with the experimental data of Blankson [20] (see below). The solution for the finest mesh of 135×58 grid points differs by only 5% in stagnation point location from the 92×58 mesh solution. The axial distributions of other variables are almost identical between these two meshes. Therefore, the latter mesh was adopted for most of the computations.

Findings

Wake Shock. The wake shock can be visualized in Fig. 5, by reversals in the constant-density contours. Inspection of all the computations shows that the origin of the shock lies between 1 and 1.3 base diameters downstream of the base, independently of Mach and Reynolds numbers. The location of this point is of some importance, because it is easily recognizable in photographs of free-flight experiments, and it might be used as a reference for other features of the wake structure, such as the location of the rear stagnation point. The wake simulations of Reklis and Conti[33] at Mach 6.32 indicated no correlation between the origin of the wake shock and the location of the rear stagnation point, because the former is insensitive to Reynolds number, but not so the latter. The present investigation confirms these conclusions for Mach 4.32 and 6.32 but, as indicated below, it shows that at Mach 10 the rear stagnation point becomes insensitive to Reynolds number, and its axial location is indeed close to the origin of the wake shock.

Rear Stagnation Point. The rear stagnation point is at the downstream end of the recirculation region, and it indicates the axial extent of the slow, recirculating flow. The wake flowfield is visualized in Fig. 6 by the velocity fields and streamlines, for selected Mach and Reynolds numbers. The results shown in that figure for Mach 4.32 and 6.32 suggest that in supersonic and low hypersonic flow the position of the rear stagnation point is sensitive to Mach and Reynolds numbers: increasing the Mach number moves the stagnation point closer to the base, whereas increasing the Reynolds number moves it away from the base. However, at Mach 10 the location of the stagnation point is insensitive to Reynolds number. This is illustrated in Fig. 7, which compares all the present results with the measurements by McLaughlin[18] and Blankson[20], and the correlation by Martellucci *et al*[25]. The vertical bars represent the uncertainty in the McLaughlin and Blankson experiments at Reynolds 94,000 and 86,000 respectively. The present computations at Reynolds 86,000 fall within these uncertainty limits, and are considered to agree with the experimental data. The disagreement reported by Reklis and Conti[33] between their early results and the Blankson data has been traced by the present investigators to lack of sufficient grid resolution in the early wake simulations. The hypersonic correlation by Martellucci *et al*, as well as the shape of the curve faired through the present results in Fig. 7, suggest that at Mach 10 and beyond, the location of the rear stagnation point lies at approximately one base diameter downstream of the base, independently of Mach and Reynolds numbers.

Flow Separation. Several investigators (*e.g.* Donaldson[26], Kayser[27,28]) have reported flow separation taking place beyond sharp or rounded corners, on the base itself. In order to investigate this phenomenon, the present numerical simulations were conducted with sufficient grid resolution near the base to establish the location of the flow separation line. A typical base-flow velocity field is shown on Fig. 8, where the location of the separation line (indicated by an arrow) has been interpolated between two mesh points. The results of all the present computations are plotted in Fig. 9 as a function of Mach number. There is a clear trend for the separation line to move away from the corner, towards the axis, with increasing Mach number. At Mach 4.32 and 6.32, increasing the Reynolds number moves the separation line outwardly towards the corner. At Mach 10 the separation line is insensitive to Reynolds number.

Axial Velocity. Typical plots of axial-velocity distribution along the axis of symmetry are shown on Fig. 10. Near the base the axial velocity goes through a minimum, beyond which it increases asymptotically to its far-field value. The location of the minimum shows a weak dependence on the Mach and Reynolds

numbers, and it correlates well with the axial location of the center of rotation of the recirculating flow, as shown graphically on Fig. 8. This correlation is plotted in Fig. 11, where all but one of the data points fall within a $\pm 15\%$ error band. The good correlation is attributed to the fact that in the low-speed environment of the wake the rotating flow imposes the pressure of its core, and the corresponding speed, on the wake axis.

Axial Distribution of Static Pressure. Typical distributions of static pressure along the wake axis are shown on Fig. 12. Two features of the pressure distribution are the minimum associated with the velocity minimum discussed above and, in some cases, an overshoot of the static pressure beyond the free-stream value, which it should approach asymptotically in the far field. McLaughlin[18] pointed out that the overshoot is greater at lower Mach number, and the present results confirm this statement.

Base Pressure. Figure 13 shows a plot of the wall pressure at the center of the base, taken as representative of the base pressure. Some radial variation of base pressure was observed in the numerical simulations, consisting mostly of a decrease in pressure from the center of the base towards the corner. The computed results show considerable scatter, a situation that is typical of other studies (logarithmic scales are widely used to plot base pressure). No clear trend with Mach or Reynolds numbers emerges from the computations, but the results are in general agreement with the extrapolated data reported by McLaughlin and Blankson (*loc. cit.*). In connection with extrapolating to the wall the pressures measured or computed in the flowfield to obtain base pressure, it should be noted that considerable pressure gradients exist near the wall, as shown in Fig. 12.

Conclusions

- Numerical simulations of hypersonic wakes show good qualitative agreement with experimental data. Major flow features show good quantitative agreement.
- The wake flow separates on the base of the cone, between the sharp corner and the axis of symmetry.
- The axial velocity has a minimum near the base. Its location correlates with the location of the core of the recirculating flow.
- The static pressure on the axis overshoots its free-stream value, particularly at low Mach number.
- Mach number effects:
  Increasing the Mach number from 4 to 10 has a significant effect on
  -Shortening the recirculation region
  -Shifting the separation line towards the axis
  And a weak effect on
  -Base pressure
  -Origin of the wake shock.
- Reynolds number effects: At Mach 4 and 6, increasing the Reynolds number lengthens the recirculation region, and shifts the separation line towards the base corner. At Mach 10, Reynolds number effects are negligible.

Acknowledgments

This research was sponsored by the U.S. Office of Naval Research, under Contract No. N00014-82-C-0690. The Lockheed Independent Research Program sponsored the development of computer codes used in the investigation. The authors gratefully acknowledge the useful comments of Dr. R. P. Reklis, and the operational help of Mrs. K. Neier.

References

1. R. I. Crane, "A Survey of Hypersonic Near Wake Studies", *The Aeronautical Journal of the Royal Aeronautical Society*, Vol. 73 pp. 996–1006, 1969.

2. Dean R. Chapman, "An Analysis of Base Pressure at Supersonic Velocities and Comparison with Experiment", NACA Technical Report 1051, 1951.

3. Eric Baum, "An Interaction Model of a Supersonic Laminar Boundary Layer on Sharp and Rounded Backward Facing Steps", *AIAA Journal,* Vol. 6, pp. 440–447, 1968.

4. Francis R. Hama, "Experimental Studies of the Lip Shock", *AIAA Journal,* Vol. 6, pp. 212–219, 1968.

5. John T. Ohrenberger and Eric Baum, "A Theoretical Model of the Near Wake of a Slender Body in Supersonic Flow", AIAA Paper 70-792, 1970.

6. R. F. Weiss, "A New Theoretical Solution of the Laminar, Hypersonic Near Wake", *AIAA Journal,* Vol. 5, pp. 2142–2148, 1967.

7. Seymour L. Zeiberg and Gary D. Bleich, "Finite-Difference Calculation of Hypersonic Wakes", *AIAA Journal,* Vol. 2, pp. 1396–1402, 1964.

8. S. M. Dash, "Recent Developments in the Modeling of High Speed Jets, Plumes and Wakes", AIAA Paper 85-1616, 1985.

9. John M. Cassanto, "Radial Base-Pressure Gradients in Laminar Flow", *AIAA Journal,* Vol. 5, pp. 2278–2279, 1967.

10. Bruce M. Bulmer, "Re-Entry Vehicle Base Pressure and Heat-Transfer Measurements at M = 18", *AIAA Journal,* Vol. 13, pp. 522–524, 1975.

11. W. C. Lyons, Jr., J. J. Brady and Z. J. Levensteins, "Hypersonic Drag , Stability, and Wake Data for Cones and Spheres", AIAA Paper 64–44, 1964.

12. Kenneth E. Koch, "Supersonic Cone Wake-Neck Geometry", *AIAA Journal,* Vol. 5, pp. 2087–2086, 1967.

13. Z. J. Levensteins and M. V. Krumins, "Aerodynamic Characteristics of Hypersonic Wakes", *AIAA Journal,* Vol. 5, pp. 1596–1602, 1967.

14. Bain Dayman Jr., "Support Interference Effects on the Supersonic Wake", *AIAA Journal,* Vol. 1, pp. 1921–1923, 1963.

15. R. I. Crane, "Comment on 'Measurements in the Laminar Near-Wake of Magnetically Suspended Cones at M = 6.3'", *AIAA Journal,* Vol. 15 pp. 891–892, 1977.

16. Earll M. Murman, "Experimental Studies of a Laminar Hypersonic Cone Wake", *AIAA Journal,* Vol. 7, pp. 1724–1730, 1969.

17. Carl W. Peterson, "An Experimental Study of Laminar Hypersonic Blunt Cone Wakes", *Astronautical Acta,* Vol. 15, pp. 67-76, 1969.

18. Dennis K. McLaughlin, James E. Carter, Morton Finston, and J. Alan Forney, "Experimental Investigation of the Mean Flow of the Laminar Supersonic Cone Wake", *AIAA Journal,* Vol. 9, pp. 479–483, 1971.

19. A. R. Ahmadi, and M. Finston, "Wall Temperature Effects on Laminar Wakes", AFOSR TR-75-1634, 1975.

20. Isaiah M. Blankson, and Morton Finston, "Measurements in the Laminar Near-Wake of Magnetically Suspended Cones at M = 6.3", *AIAA Journal,* Vol. 13, pp. 1562–1567, 1975.

21. Edward M. Schmidt and Robert J. Cresci, "An Experimental Investigation of Hypersonic Flow Around a Slender Cone", Polytechnic Institute of Brooklyn Report 1031, 1967.

22. J. M. Cassanto, "A Base Pressure Experiment for Determining the Atmospheric Pressure Profile of Planets", *J. Spacecraft,* Vol. 10, pp. 253–261, 1973.

23. F. Browand, M. Finston, and D. McLaughlin, "Wake Measurements Behind a Cone Suspended Magnetically in a Mach Number 4.3 Stream", AGARD CP 19, 1967.

24. Hartmut H. Legner and Michael L. Finson, "Mach Number Dependence of Laminar Near-Wake Transition for Slender Cones", *AIAA Journal*, Vol. 3 pp. 417-484, 1977.

25. A. Martellucci, H. Trucco, and A. Agnone, "Measurements of the Turbulent Near Wake of a Cone at Mach 6", *AIAA Journal*, Vol. 4 pp. 385-391, 1966.

26. I. S. Donalson, "On The Separation of a Supersonic Flow at a Sharp Corner", *AIAA Journal*, Vol. 5 pp 1086-1088, 1967

27. L. D. Kayser, " Oil Flow Studies of Base Separation at Supersonic speed ", BRL -R 1809

28. L. D. Kayser, " Experimental Study of Separation From the Base of a Cone at Supersonic Speeds", BRL-AD/A-005 015

29. J. Sahu, C. J. Nietubicz, and J. L. Steger, "Numerical Computation of Base Flow for a Projectile at Transonic Speeds", AIAA Paper 82-1358, 1982.

30. G. S. Deiwert, "Three-Dimensional Flow Over a Conical Afterbody Containing a Centered Propulsive Jet: A Numerical Simulation", AIAA Paper 83-1709, 1983.

31. P. D. Thomas, R. P. Reklis, R.R. Roloff and R.J. Conti, "Numerical Simulation of Axisymmetric Base Flow on Tactical Missiles with Propulsive Jet", AIAA Paper 84-1658, 1984.

32. R. P. Reklis, R. J. Conti, and P. D. Thomas, "Numerical Simulation of Hypersonic Viscous Flow Over Cones at Very High Incidence", AIAA Paper 83-1669, 1983.

33. R. P. Reklis, and R. J. Conti, "Computational Probing of Hypersonic Laminar Wakes", AIAA Paper 84-1579, 1984.

34. P. D. Thomas, "Numerical Method for Predicting Flow Characteristics and Performance of Nonaxisymmetric Nozzles—Theory", NASA Contractor Report No. 3147, September 1979.

35. C. J. Nietubicz, T. H. Pulliam and J. L. Steger, "Numerical Solution of the Azimuthal-Invariant Thin-Layer Navier-Stokes Equations", AIAA Paper 79-0010, 1979.

36. T. H. Pulliam and J. L. Steger, "On Implicit Finite-Difference Simulations of Three-Dimensional Flow", AIAA Paper 78-10, 1978.

37. R. Beam and R. F. Warming, "An Implicit Factored Scheme for the Compressible Navier-Stokes Equations", AIAA Paper 77-645, 1977.

38. P. D. Thomas and C. K. Lombard, "The Geometric Conservation Law–A Link Between Finite-Difference and Finite-Volume Methods of Flow Computation on Moving Grids", AIAA Paper 78-1208, 1978.

39. E. Waldbusser, "Geometry of the Near Wake of Pointed and Blunt Hypersonic Cones", *AIAA Journal*, Vol. 4, pp. 1874-1876, 1966.

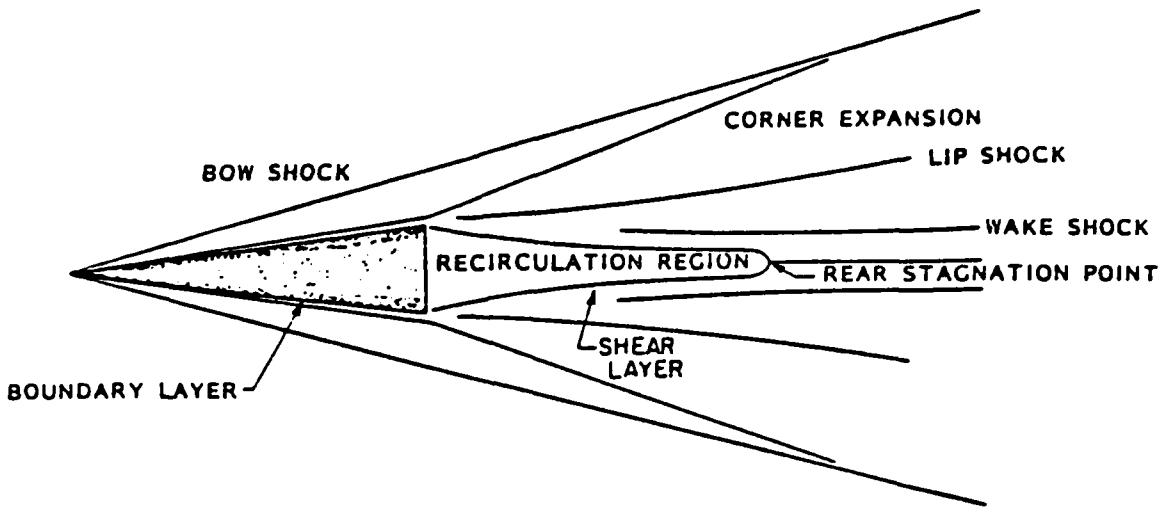

Fig. 1. Typical structure of the near wake of a cone in hypersonic flight.

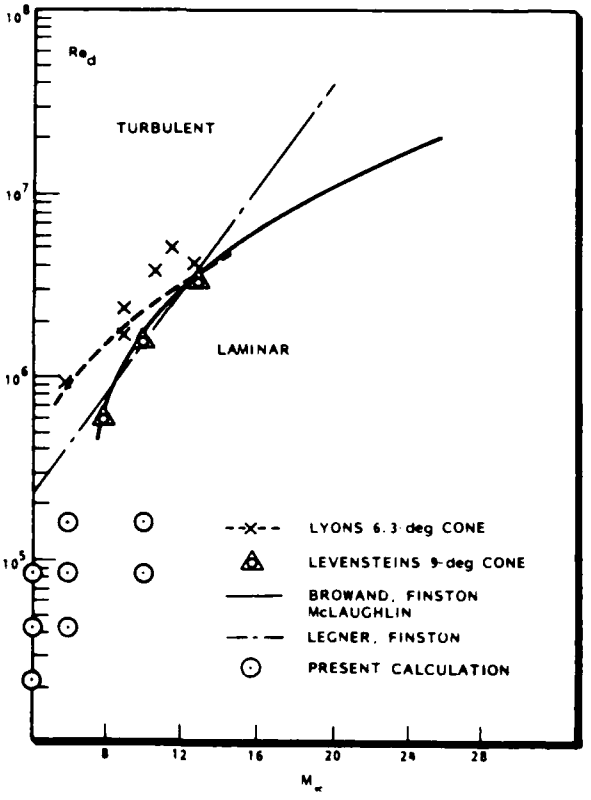

Fig. 2. The Reynolds number at which transition occurs one diameter downstream of the base, as a function of Mach number. Reference parameters are the free stream and the base diameter.

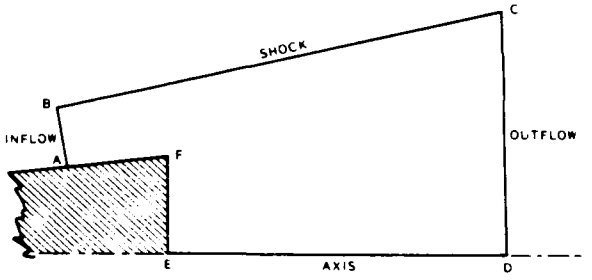

Fig. 3. Topology of the physical domain and boundary conditions for wake computations.

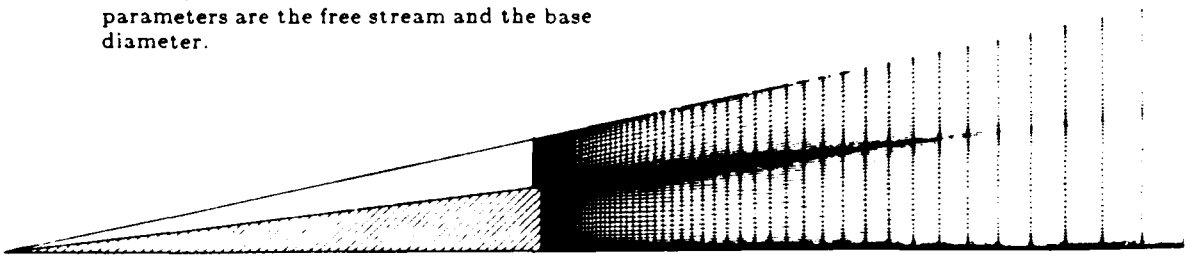

Fig. 4. Typical mesh for wake computations, with 92 (axial) × 58 (radial) nodes.

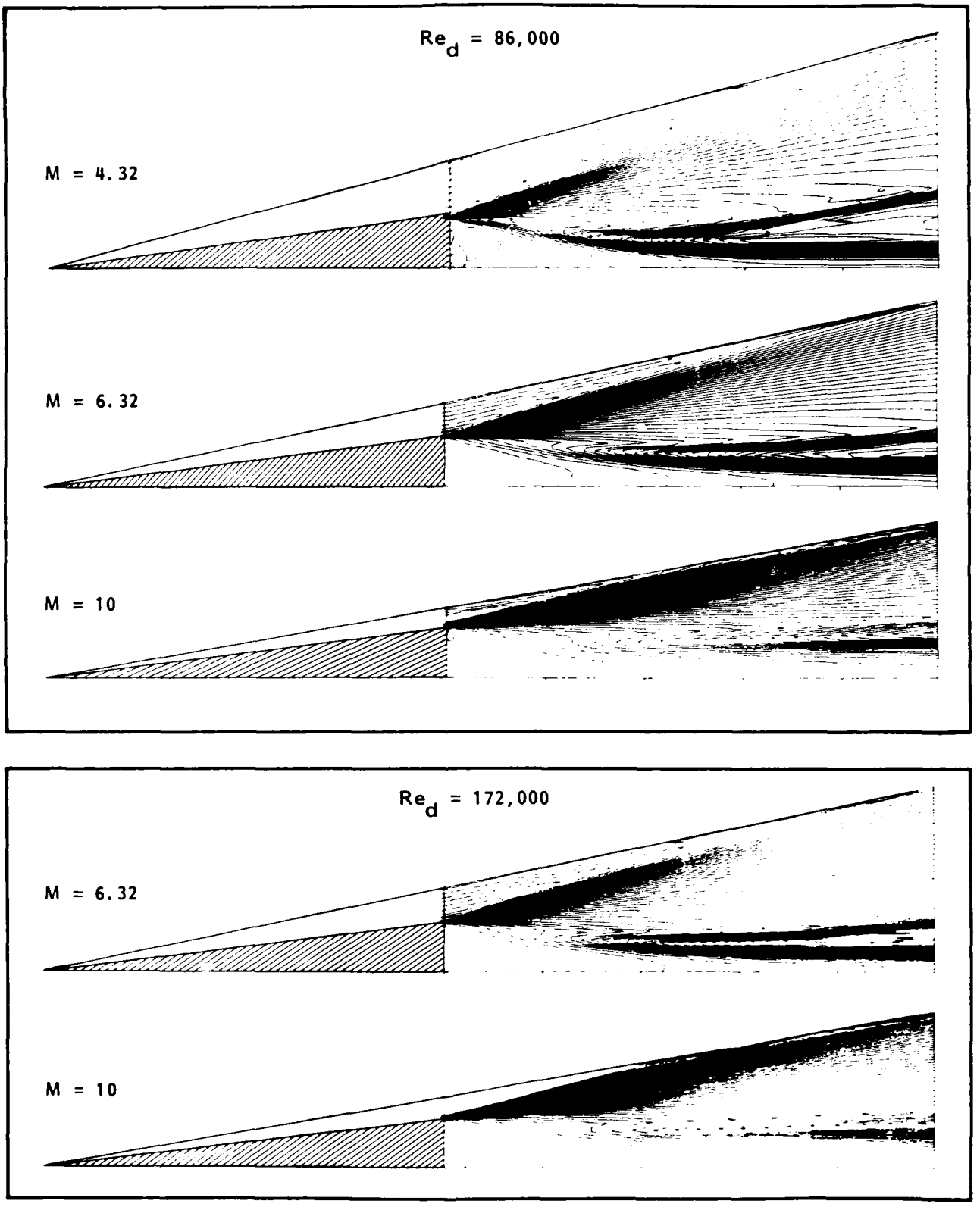

Fig. 5. Constant-density contours in the near wake, for selected Mach and Reynolds numbers.

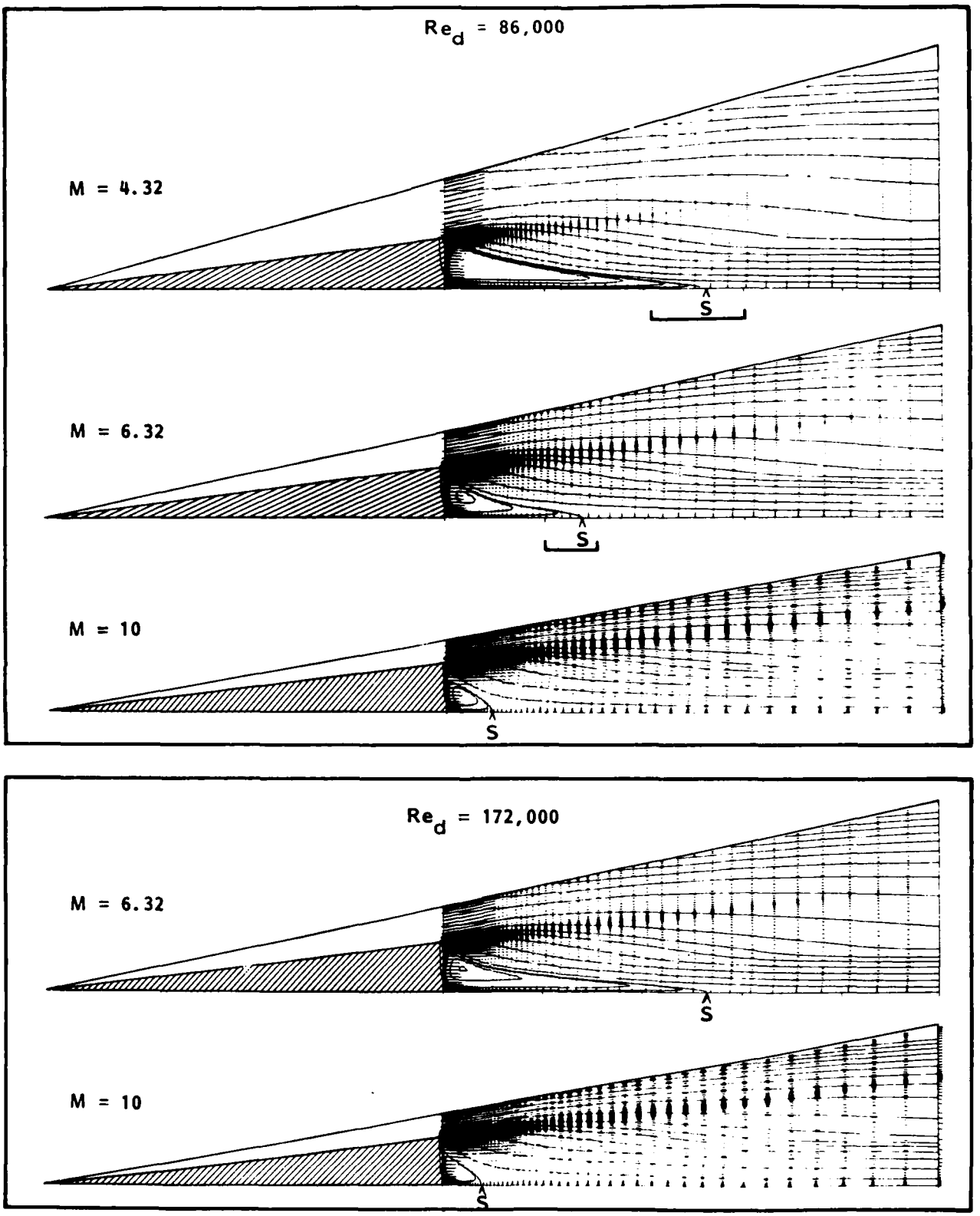

Fig. 6. Velocity field and streamlines in the near wake, for selected Mach and Reynolds numbers. The computed location of the rear stagnation point is labelled "S"; experimental values are indicated by the bars.

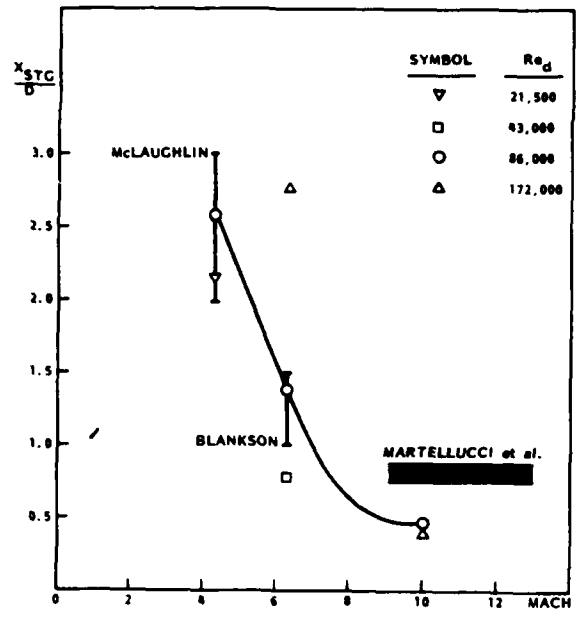

Fig. 7. Axial location of the rear stagnation point downstream of the base, normalized by the base diameter. Vertical bars indicate the range of experimental values. The horizontal bar represents a correlation of hypersonic experimental data.

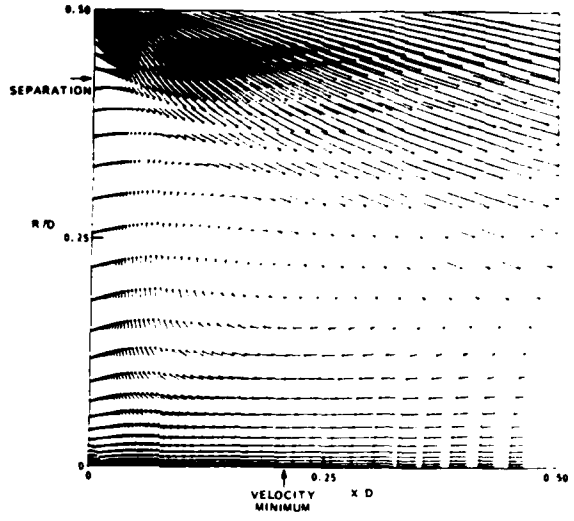

Fig. 8. Velocity field near the base, for Mach 6.32 and Reynolds 86,000. Radial (**R**) and axial (**X**) coordinates are normalized by the base diameter.

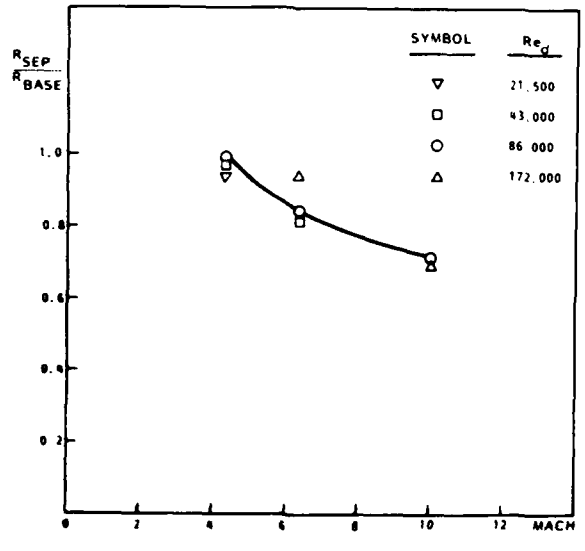

Fig. 9. Radial location of the flow separation line on the base, as a function of Mach number, for a range of Reynolds number.

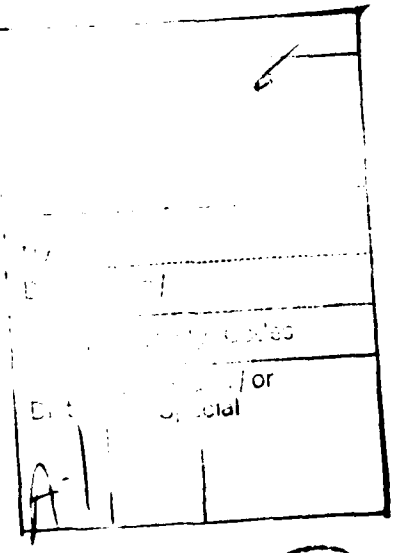

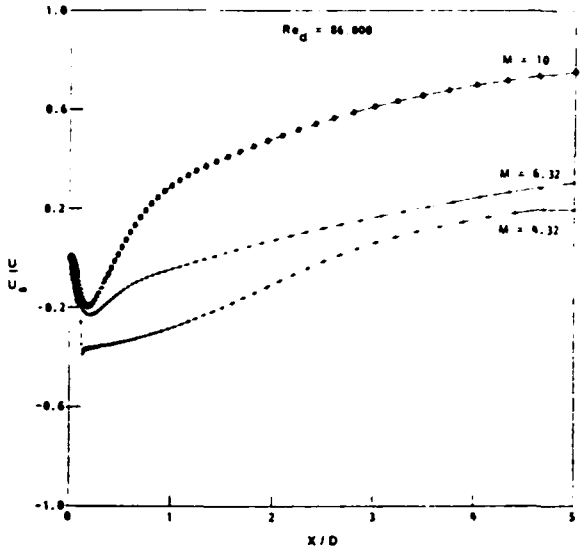

Fig. 10. Effect of free-stream Mach number on the axial-velocity distribution along the axis of symmetry.

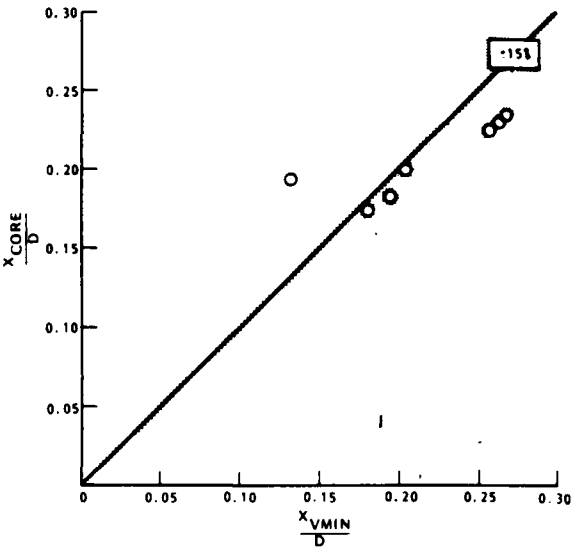

Fig. 11. Correlation between the axial location of the core of the recirculating flow (center of rotation) and that of the minimum axial velocity.

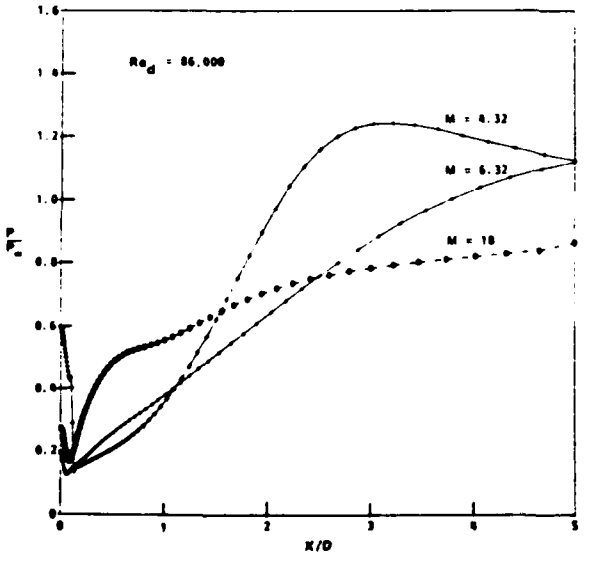

Fig. 12. Effect of free-stream Mach number on the static pressure distribution along the axis of symmetry.

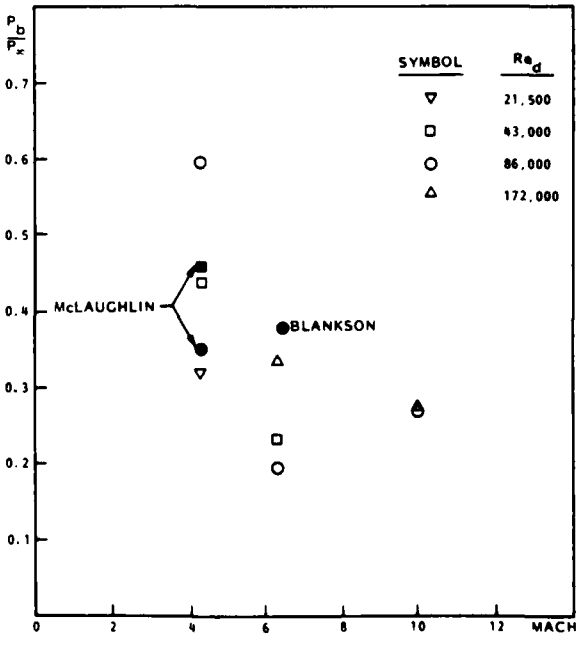

Fig. 13. Base pressure normalized by free-stream static pressure. Filled-in symbols indicate experimental data.

END

FILMED

12-85

DTIC